수중 SAW Device의 최적 설계법

Optimal Design of Underwater SAW Devices

노 용 래*

(Yong Rae Roh)

요 약

최근 신호 처리 기기와 센서로서 각광을 받고 있는 SAW Device는 때론 목적에 따라 수중에서 사용해야 할 때가 있다. 그러나 유체내의 고체 표면을 전파하는 표면파의 경우, 유체내로의 에너지 손실로 인해 설계상에 많은 어려움을 주고 있다. 따라서 본 연구에서는 이러한 어려움을 극복할 수 있는 최적 설계법으로서, 컴퓨터 모형해석을 통해 수중에서 압전 물질에 의한 표면파의 최대 발진 효율, 최소 전파 감쇄율, 그리고 pure mode 전파를 이룰 수 있는 SAW Device의 최적 geometry, 즉 초적 압전 결정 형면, 표면파 전파 방향, 그리고 무차원 전파 계수 높을 구하였다. 본 논문에서는 표면파가 전파하는 고체 재료로서 PZT와 PVDF 적층, 그리고 쇠 하부층을 사용하였으나, 이 설계법은 임의의 유체층과 고체층의 조합에도 적용할 수 있다. 동일한 기술은 수중음향 계측기, antifouling, 그리고 산업 및 의료 분야 등에 쓰이는 센서와 엑신기의 설계에도 바로 응용할 수 있다.

ABSTRACT

Depending on purpose, SAW device may have to funciton while immersed in a liquid. Those who are familiar with SAW devices would anticipate difficulty since the propagating surface waves will tend to radiate energy into the liquid and hence suffer attenuation. Thus, to design an immerable SAW device, more attention and full information about the wave properites is required to overcome the attenuation and get the highest SAW generation eficiency. Through numerical simulation, the optimal geometry of underwater SAW devices, such as optimal piezoelectric crystal cut, SAW propagation direction and nondimensional wave number(ka) is determined to get the maximum SAW excitation efficiency, the minimum attenuation in propagation and pure mode propagation for all the modes of surface wave propagation. The design technique can be applied to an arbitrary combination of a piezoelectric layer, a substrate and a liquid medium. In this paper, PZT and PVDF layers and a steel substrate are use for the solid medium. The technique can be easily employed for the design of underwater sensors and actuators for the applications, such as sonar, marine antifouling, industrial and medical uses.

* 산업과학기술연구소

Ⅰ. Introducton

For several decades, bulk elastic waves propagating inside solids have played an important role in electronics. Initially these waves were used in oscillators and filters employing precisely dimensioned piezoelectric crystals, usually made from quartz[1]. Later, devices which employed the propagation of bulk elastic waves in solids over paths that were many wavelengths long, were made for the guidance or delay of signals. Recently, engineers in many different fields have directed attention to surface elastic waves because of the possibility of constructing signal processing devices which employ these waves and their superiority to bulk wave devices. These waves are modes of propagation of elastic energy along the free surface of an infinite half-space in which the displacement amplitudes of the propagating waves decay in an exponential fashion with depth beneath the surface. Hence, essentially all of the associated energy density is concentrated within a distance of the order of a wavelength below the free surface. Devices employing the surface waves, SAW devices, have found various uses and intensive research activity has had rapid results in terms of applications to the consumer, commercial and military markets[2]. Depending on purpose, SAW devices may have to function while immersed in a liquid. Those who are familiar with SAW devices would anticipate difficulty since the propagating surface waves would tend to radiate energy into the liquid and hence suffer attenuation. Viktorov's study[3] suggests that losses around 4 dB/MHz cm will arise. But the experimental loss-free results of Roederer and Bastiaans[4] and of Bastiaans[5] prove the feasibility of an immersable SAW device, yet the device should be designed more carefully to overcome the attenuation in propagation. Therefore an accurate and reliable design method needs to be developed for the underwater SAW devices.

In designing underwater SAW device, there are several factors which should be considered carefully. The first is the SAW generation efficiency by means of IDTs. Piezoelectricity, utilized in a SAW device, is the phenomenon which couples elastic stresses and strains to electric fields and displacements. It occurs only in anisotropic materials whose internal structure lacks a centre of symmetry. Because of the inherent anisotropy, the SAW generation efficiency by IDTs is different for different materials, crystal cuts, SAW propagation directions and types of the surface waves. Thus it should be carefully studied and, for a given material and type of the surface waves, the optimal combination of the variables should be selected to get the highest generation efficiency. The most convenient way to find the combination is to calculate SAW velocities with electrically open and shorted boundary conditions at the free surface of the piezoelectric layer and to compare the fractional change of the two sets of values. If no change occurs under such a boundary condition change, the interaction between the surface waves and the perfect conductor at the top of the piezoelectric layer is negligible so far as surface wave generation is concerned. On the other hand, if the change in velocity is significant, the interaction between the surface waves and an electrode type transducer should be correspondingly greater. Therefore with the two sets of velocity data, the value of $\Delta v/v$ (v : phase velocity with open electrical boundary conditions, v' : phase velocity with shorted electrical boundary conditions, $\Delta v = v - v'$) is calculated in order to estimate the surface wave excitation efficiency by means of interdigital electrode transducers[6].

The next factor is that the surface wave prop

agation should be a pure mdoe. In otner words, the direction of the waves' energy flow should coincide with the direction of the wave propagation [7]. Unless the propagating wave is a pure mode, it is very likely that, in the SAW device, the waves generated by a transmitter may totally miss a receiver. Especially, for a large low frequency SAW device, this factor should be carefully treated. Therefore only the piezoelectric crystal cut and propagation direction showing a pure mode propagation should be employed in the design of the device.

Another and the most important factor is the attenuation in propagation. The attenuating property of the underwater surface waves should be studied in detail, and based on the results, the crystal cut, the propagation direction, the nondimensional wave number ka for a given material, and the type of surface waves having the minimum attenuation in propagation should be selected.

Considering all these factors, the optimal geometry of underwater SAW devices should be determined so that the maximum SAW generation efficiency, the minimum propagation attenuation and pure mode propagation can be achived.

The surface wave propagation at the boundary between a fluid and a solid medium has been investigated by some authors[3, 8] both theoretically and experimentally. But those works are concerned only with the Rayleigh wavs when the solid medium is isotropic and nonpiezoelectric. Furthermore, higher mode Rayleigh waves (2nd, 3rd…) were not paid much attention, and therefore, the underwater SAW propagation is not as well understood as the traction free SAW propagation. In this paper, all the possible surface acoustic wave propagation at the boundary between a fluid medium (water) and a layered medium of thin film of piezoelectric material on an infinite isotropic half space), shown in Fig. 1, is investigated extensively through numerical analysis. When the SAW frequency is high, the piezoelectric layer itself can be considered as an infinite half space in comparison with the wavelength of surface waves, while the existence of the substrate under the layer can be ignored. However when the frequency is low, the thickness of the piezoelectric layer becomes less than the wavelength and the influence of the substrate can no longer be ignored [9]. Therefore, the general surface acoustic wave propagation in a thin film of piezoelectric material on an infinite isotropic half space is investigated for the development of both high and low frequency SAW devices.

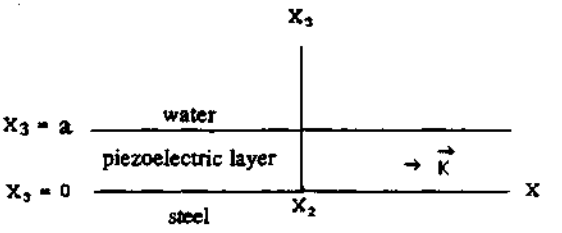

Fig. 1 Coordinate system for surface wave propagation in a thin layer of piezoelectric material on steel

For all the piezoelectric crystal cuts where surface wave propagation is of pure mode, two-dimensional and three-dimensional dispersion curves of all the types of surface waves are calculated for all the modes of propagation. All the first mode surface wave velocities are calculated with both open and shorted electrical boundary conditions at the layer surface. In addition, the attenuation of the surface waves in the propagation direction is calculated and described. Based on the results, by considering the design factors mentioned above, the optimal geometry of the immersed SAW device is obtained for each type of surface waves. The optimal geometry means optimal crystal cut, propagation direction and nondimensional wave number ka. In the calculations, for the infinite isotropic half space substrate, steel is used and for the piez-

oelectric layer, PZT-5H is used for the general investigation of a SAW propagation in arbitrary piezoelectric crystal cuts. Later, the general technique developed with PZT-5H is applied to PVDF. For PVDF, because of its availability only as a thin film, only the crystal XY plane is used as the layer[10].

Ⅱ. Caculation Procedure

This section formulates the general problem of underwater surface wave propagation on a layerd medium. The coordinate system to be used throughout the discussion is illustrated in Fig. 1. The wave number k is made to be a complex number (k_r+ik_i) to represent the attenuation in the propagation direction. The imaginary part of $k(k_i)$ will be the attenuation factor in propagation. The propagation direction denoted by the wave number k is taken as the X_1 direction. The surface waves decay in the negative X_3 direction. For the representation of different cuts of surface plane and propagation directions, arbitrary orientations of the crystal surface with respect to the coordinate axes (X_1, X_2 and X_3) are considered. This is carried out by means of a coordinate transformaion through Euler angles from the crystal axis to the desired coordinate system. For surface acoustic wave propagation on a piezoelectric material, due to the low velocity of he waves relative to electromagnetic wave velocities, magnetic fields can be neglected and electric fields are derived from a scalar potential. With this quasi static approximation, in the solid medium, the displacements U_j and the electric potential ϕ in each medium satisfy the following equations of motion, respectively[11]

$$\rho\frac{\partial^2 U_j}{\partial t^2} - C_{ijkl}\frac{\partial^2 U_k}{\partial x_i \partial x_l} - e_{kij}\frac{\partial^2 \phi}{\partial x_i \partial x_k} = 0$$

$$e_{ikl}\frac{\partial^2 U_k}{\partial x_i \partial x_l} - \varepsilon_{ik}\frac{\partial^2 \phi}{\partial x_i \partial x_k} = 0 \quad , \tag{1}$$

where ρ is the density of the medium, C_{ijkl} is the elastic stiffness tensor measured at constant electric field, e_{kij} is the piezoelectric tensor and ε_{ik} is the dielectric tensor measured at constant strain. For the substrate, because the material (steel) is an isotropic and conducting material, the piezoelectric constants are zero and the electric potential in Eq. 1 is ignored. All the data used are from Auld[7].

For each medium, the elastic displacement U_j and the electric potential ϕ are assumed to be a linear combination of terms or partial waves of the following form:

$$\begin{aligned} U_j &= \alpha_j \exp(ikbx_3)\exp[i(kx_1 - \omega t)] \\ \phi &= \alpha_4 \exp(ikbx_3)\exp[i(kx_1 - \omega t)] \end{aligned} \quad , \tag{2}$$

where α_j is the relative amplitude factor, b is the decay factor and ω is the frequency. When the assumed solutions are substituted into Eq. 1, the relations between ω / k, b and α_j of the PZT-5H layer are obtained through Eq. 3:

$$\begin{bmatrix} M_{11}-\rho(\frac{\omega}{k})^2 & M_{12} & M_{13} & M_{14} \\ M_{12} & M_{22}-\rho(\frac{\omega}{k})^2 & M_{23} & M_{24} \\ M_{13} & M_{23} & M_{33}-\rho(\frac{\omega}{k})^2 & M_{34} \\ M_{14} & M_{24} & M_{34} & M_{44}-\rho(\frac{\omega}{k})^2 \end{bmatrix} \begin{bmatrix} \alpha_1 \\ \alpha_2 \\ \alpha_3 \\ \alpha_4 \end{bmatrix} = 0 \tag{3}$$

where

$$\begin{aligned} M_{11} &= C_{55}b^2 + 2C_{15}b + C_{11} \\ M_{33} &= C_{33}b^2 + 2C_{35}b + C_{55} \\ M_{13} &= C_{35}b^2 + (C_{13}+C_{55})b + C_{15} \\ M_{14} &= e_{35}b^2 + (e_{15}+e_{31})b + e_{11} \\ M_{34} &= e_{33}b^2 + (e_{13}+e_{35})b + e_{15} \\ M_{22} &= C_{44}b^2 + 2C_{46}b + C_{66} \\ M_{12} &= C_{45}b^2 + (C_{14}+C_{56})b + C_{16} \end{aligned}$$

$$M_{23} = C_{34}b^2 + (C_{36} + C_{45})b + C_{56}$$
$$M_{24} = e_{34}b^2 + (e_{14} + e_{36})b + e_{16}$$
$$M_{44} = -(\varepsilon_{33}b^2 + 2\varepsilon_{13}b + \varepsilon_{11}).$$

For the steel substrate, an equation similar to Eq. 3 is obtained, except that all terms involving piezoelectric constants and permittivities are absent.

For a nontrivial solution, the determinant of the coefficient matrix in Eq. 3 should be zero. The determinant is an algebraic equation in the quantity ω/k, and b which gieves the depth dependence of the waves. For a certain assumed value of ω/k, eight roots are obtained for b in the layer, and six are obtained for the substrate. Of the six roots calculated for the substrate, only those having a negative imaginary part are acceptable, since the waves decay and vanish at infinite depth. For the layer of finite thickness, the waves may grow, decay or remain constant: all the eight roots are admissible. Hence, for the solid layered medium under consideration, eleven partial waves (three for steel, eight for piezoelectric layer) are combined together with the weighting factros (α_j) denoting relative amplitude ratios. In the layer,

$$U_j = \left[\sum_{n=1}^{8} A_n \alpha^{(n)}{}_j \exp(ikb^{(n)}x_3)\right] \exp[i(kx_1 - \omega t)]$$
$$\phi_j = \left[\sum_{n=1}^{8} A_n \alpha^{(n)}{}_4 \exp(ikb^{(n)}x_3)\right] \exp[i(kx_1 - \omega t)],$$

in the substrate,

$$U'_j = \left[\sum_{m=1}^{3} A_m \alpha'^{(m)}{}_j \exp(ikb'^{(m)}x_3)\right] \exp[i(kx_1 - \omega t)] \quad (4)$$

where A_n and A_m are other relative amplitude weighting factors to be determined using boundary conditions.

In water, the particle displacements and electric potential are assumed to have the following form

$$U''_1 = \alpha_1 \exp(ikb_w x_3) \exp[i(kx_1 - \omega t)]$$
$$U''_3 = \alpha_3 \exp(ikb_w x_3) \exp[i(kx_1 - \omega t)]$$
$$\phi'' = \alpha_4 \exp(ikb_w x_3) \exp[i(kx_1 - \omega t)]. \quad (5)$$

The elastic property of water is represented by a single elastic constant λ(modulus of compression) while the effect of viscosity is ignored. The assumed solutions satisfy the following equations of motion simplified from general equations[12] :

$$\frac{\partial^2 U''_1}{\partial x_1{}^2} + \frac{\partial^2 U''_3}{\partial x_1 \partial x_3} = \frac{\rho_w \partial^2 U''_1}{\lambda \partial t^2}$$
$$\frac{\partial^2 U''_1}{\partial x_1 \partial x_3} + \frac{\partial^2 U''_3}{\partial x_3{}^2} = \frac{\rho_w \partial^2 U''_3}{\lambda \partial t^2}$$
$$\nabla^2 \phi'' = 0, \quad (6)$$

where ρ_w is the density of water. Substitution of U''_1 and U''_3 into Eq. 6 leads to the following equation :

$$\begin{bmatrix} 1 - \frac{\rho_w}{\lambda}\left(\frac{\omega}{k}\right)^2 & b_w \\ b_w & b_w{}^2 - \frac{\rho_w}{\lambda}\left(\frac{\omega}{k}\right)^2 \end{bmatrix} \begin{bmatrix} \alpha_1 \\ \alpha_3 \end{bmatrix} = 0 \quad (7)$$

To have a nontrivial solution, the determinant of the coefficient matrix in Eq. 7 should be zero. From which it follows that

$$b_w^{(1)} = +\sqrt{-1 + \frac{\rho_w}{\lambda}\left(\frac{\omega}{k}\right)^2},$$
$$b_w^{(2)} = -\sqrt{-1 + \frac{\rho_w}{\lambda}\left(\frac{\omega}{k}\right)^2}. \quad (8)$$

Of these two roots, a proper one is selected using the condition that the surface waves are bounded as $X_3 \to \infty$. Then the relative amplitude ratio α_3/α_1 is obtained from the Eq. 7 which is related to

of Eq. 7,

$$\alpha_1 = \frac{\lambda b_w}{\rho_w\left(\frac{\omega}{k}\right)^2 - \lambda}\alpha_3 \tag{9}$$

Then the displacements in water are determined by Eq. 10 :

$$U''_1 = C\alpha_1 \exp(ikb_w x_3)\exp[i(kx_1 - \omega t)]$$
$$U''_3 = C\alpha_3 \exp(ikb_w x_3)\exp[i(kx_1 - \omega t)], \tag{10}$$

where C is another amplitude weighting factor to be determined using boundary conditions. Now, with the constitutive equations of a piezoelectric medium (Eq. 11), the boundary conditions at the interface between the piezoelectric layer and the steel, as well as the layer and water are applied to the sets of solutions of each medium. The constitutive equations are

$$T_{ij} = C_{ijkl}S_{kl} - e_{kij}E_k$$
$$D_i = \varepsilon_{ik}E_k + e_{ikl}S_{kl}, \tag{11}$$

where T_{ij} is the stress, S_{kl} is the strain, E_k is the electric field and D_i is the electric displacement. The boundary conditions are

(a) Mechanical Transverse

(1) continuity of transverse displacement at the interface between layer and substrate : $U_2 = U'_2$

(2) continuity of transverse shear traction at the interface between layer and substrate : $T_{32} = T'_3$

(3) vanishing of transverse shear traction at the interface between water and layer, $T_{32} = 0$

(b) Electrical

(4) continuity of the normal electric displacement at the interface between layer ad substrate : $D_3 = D'_3$

(5) continuity of electric potential at the interface between layer ad substrate : $\phi = \phi'$

(6) continuity of the normal electric displacement at the interface between water and layer : $D_3 = D''_3$

(7) continuity of electric potential at the interface between water ad layer : $\phi = \phi''$

(c) Mechanical Sagittal

(8) continuity of longitudinal displacement at the interface between layer and substrate : $U_1 = U'_1$

(9) continuity of vertical displacement at the interface between layer and substrate : $U_3 = U'_3$

(10) continuity of sagittal shear traction at the interface between layer and substrate : $T_{31} = T'_5$

(11) continuity of normal traction at the interface between layer and substrate : $T_{33} = T'_3$

(12) vanishing of sagittal shear traction at the interface between water and layer, $T_{31} = 0$

(13) continuity of normal traction at the interface between water and layer : $T_{33} = T''_3$

(14) continuity of vertical displacement at the interface between water and layer : $U_3 = U''_3$

where U, T, D, ϕ are of the layer, U', T' are of the substrate and U'', D'', T'', ϕ'' are of the free space, respectively. Since the substrate material is a conductor, ϕ' at the interfae between the layer and the substrate is zero. Hence, in composing a boundary condition matrix, the conditions (4) and (5) are combined through row reduction. In addition, the form of the potential in water is taken to be

$$\phi'' = \phi_a \exp[-k(x_3 - a)] \tag{12}$$

where ϕ_a is the electric potential in the layer at the interface with water, to satisfy both Laplace's Equation and the boundary condition (7). Because $D_3 = -\varepsilon(\partial\phi'/\partial X_3)$, by setting $D_3 = k\varepsilon\phi$ at the layer surface, the conditions (6) and (7) are also combined. The total number of remainging boundary conditions is twelve. The unknown relative amplitude weighting factors C_i and α_i are also

twelve (eight for the layer, three for the substrate and one for water). Thus a 12×12 boundary condition matrix is composed, whose elements are functions of ω and complex nondimensional wave number $ka(k_ra+ik_ja)$. To get a nontrivial solution, the determinant of the coefficient matrix should be zero. For one given variable (for instance ω), the determinant contains two unknows (k_ra and k_ja). Hence the search for the roots of k_ra and k_ja is solved as a two-dimensional minimization problem. In this manner, two-dimensional and three-dimensional dispersion curves are drawn for various piezoelectric crystal cuts and SAW propagation directions in which the wave propagation is proved to be pure mode. Two-dimensional and three-dimensional curves showing k_ja/k_ra (loss factor) vs. k_ra are drawn as well. Since the complex wave number k is defined, the weighting factors A_n, A_m and C of the partial waves are obtained by calculating the eigenvectors of the boundary condition matrix. With the calculated values of b, k, α, A_n, A_m and C, the elastic displacements and electric potential of each medium are completely evaluated, except for an arbitrary factor dependent on excitation which multiplies the whole solution.

To calculate the surface wave phase velocity with shorted electrical boundary conditions at the interface between water and the layer, the layer surface is assumed to be covered by an infinitesimally thin conductor. Because the new conductor layer is so thin, the mechannical boundary conditions at the layer surface are still valid. However the potential at the layer surface is set to zero. In the same manner as before, dispersion curves are drawn with the electrically shorted boundary conditions.

III. Results

In calculation, for the piezoelectric layer, PZT-5H is used for the general investigation of a SAW propagation in arbitrary piezoelectric crystal cuts. Later, the general technique developed with PZT-5H is applied to PVDF. For the medium configuration under consideration, there are three different types of surface waves, Rayleigh, Love and Scholte waves, which can propagate simultaneously. For the Rayleigh waves, the appearance of a liquid above the solid layered medium causes them to attenuate exponentially in their propagation direction due to energy seepage into the liquid. Their wave propagation vector is inclined to the liquid and the energy of the waves is continuously transferred from the solid to the liquid medium. On the Love waves, the existence of water does not have much effect. Their wave propagation vector still lies parallel to the layer surface and there is no energy leakage into the liquid. However for certain piezoelectric layer crystal cuts, the Love waves are coupled to the electric field and because of the high dielectric constant of water, their phase velocities are changed. For the Scholte waves, which are not observed when the region above the layer is vacuum, the particle motion lies in the sagittal plane of the liquid-solid interface. Their properties of propagation have much in common with those of the Rayleigh waves. They are pure surface waves and most of their energy is confined around the interface, leaking no energy into either medium. For the Rayleigh waves, most of their energy resides in the solid part while for the Scholte waves, it resides in the water. It shows that, for the application of underwater SAW devices, the Rayleigh waves are preferred to the Scholte waves because the Rayleigh waves are more easily controlled by the circuitry on the solid medium.

The dispersion curve of the Rayleigh waves on the PZT-5H isotropic basal plane (Z-cut) propa-

in Fig. 2. On this crystal plane, the Rayleigh waves are coupled to the electric fields and they are stiffened. In the figure, solid lines denote the phase velocities of the medium under consideration and broken lines denote the results obtained when the layer surface is traction free. The fundamental mode starts at the free surface Rayleigh wave velocity of steel. When the layer surface is traction free, all the higher mode dispersion curves start at the bulk shear wave velocity of steel (v_s). But in Fig. 2, the dipersion curves of higher modes go beyond the traction free cut-off velocity (v_s). This is because the wave number is a complex number. The decay factors $b_s(m)$ with depth into the substrate are calculated from the secular equation, Eq. 3, of steel and are

$$b_s^{(1)} = b_s^{(2)} = -i\sqrt{1-\frac{\rho_s}{C_{44}}\left(\frac{\omega}{k}\right)^2}$$

$$b_s^{(3)} = -i\sqrt{1-\frac{\rho_s}{C_{11}}\left(\frac{\omega}{k}\right)^2} \qquad (13)$$

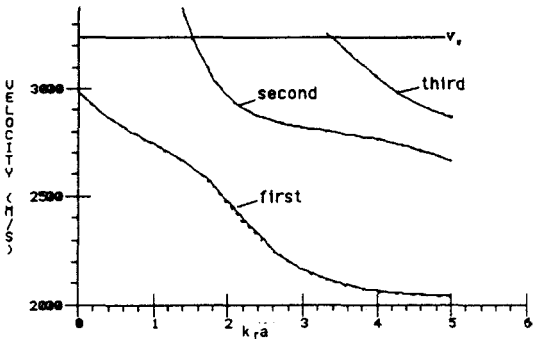

Fig. 2. Dispersion curve of Rayleigh waves on PZT 5H XY plane

where ρ_s is the density, and C_{44} and C_{11} are the elastic constants of steel. To be considered surface waves, the waves should decay with distance from the layer surface and all the b_s's should have a negative imaginary part. When k is a real number, i. e., the layer surface is traction free, at velocities higher than v_s, $b_s(1)$ and $b_s(2)$ become real numbers and the waves cease to be surface waves. But when k is a complex number, even though the value of the phase velocity (ω / real[k]) reaches v_s, unless the imaginary part of k disappears at the same time, the b_s's still maintain their negative imaginary part. The waves continue to be surface waves. The new cut-off velocities of the surface waves are the points whers b_s's cease to have negative imaginary part, which correspond to the points whre the imaginary part of k disappears. In Fig. 2, each mode starts at its own cut-off velocity where k_i becomes zero and approaches its asymptotic value. The variation of the loss factor ($k_i a / k_r a$) with $k_r a$ is shown in Fig. 3. The first mode starts at the value of 0.011 and after showing a maximum value at $k_r a = 2.3$, approaches an asymptotic value. The curve shows the minimum value at $k_r a = 0.6$. The curves of higher modes start with the $k_i a / k_r a$ value of 0 and, after maximum values, approach their asymptotic values. Within the $k_r a$ range of 0 to 5, the loss factor of the first mode is always bigger than that of higher modes. For Love waves, all three modes start at the shear wave velocity of steel and approach the unstiffened shear wave velocity of PZT-5H. The existence of the water does not make any difference becaus they are pure modes and are not coupled to electric fields. They do not leak any energy into either medium and their wave numbers are real. For Scholte waves on the isotropic basal plane, they suffer no attenuation in the propagation direction and their wave numbers are real. There is only one mdoe of propagation which starts at the Scholte wave velocity of the water-steel interface and approaches that of the water-PZT-5H interface. The velocities are always less than that of the bulk wave in the water(1477.9 m / s). When the free surface is coated with a thin layer of conductor, the phase velocities of Rayleigh waves are changed. The value of $\Delta v / v$

for the first Rayleigh mode waves, Fig. 4, reaches a local maximum at $k_r a \simeq 0.6$ and 2.6. For Love waves, since they are not coupled to the electric potential, shorting the free surface has no effect on them.

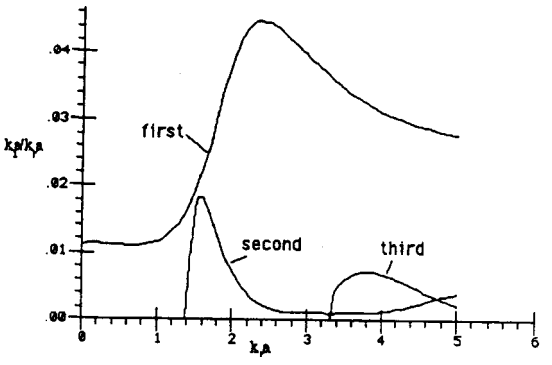

Fig. 3 Loss factor of Rayleigh waves on PZT-5H XY plane

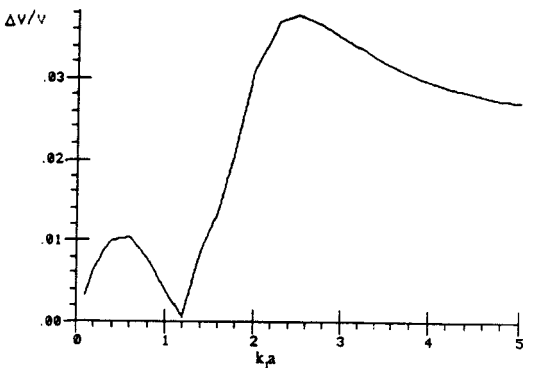

Fig. 4 Excitation efficiency vs. $k_r a$ for first mode Rayleigh waves on PZT-5H basal plane

The layer surface is changed into the crystal Y-cut plane. The isotropic basal plane becomes a vertical plane and the Z axis (poling axis) lies on the surface plane. The new surface, the crystal XZ plane, is an anisotropic plane. Therefore, the behavior of surface waves is dependent on their propagation direction. There are two pure mode propagation directions on this plane, the crystal X and Z axes. When the surface waves are propagating along the crystal Z axis, they show the same degenerate case as that on the isotropic basal plane for which the Rayleigh waves are coupled to the electric fields. For loss factors, Fig. 5, the first mode starts at the $k_i a / k_r a$ value equal to 0.011 and shows the maximum and the minimum values at $k_r a = 2.7$ and 0.7., respectively. The phase velocity of the Rayleigh waves with shorted boundary conditions at the free surface is almost the same as that with open boundary conditions. That is, coupling effect of Z axis propagation is very weak. For the Love waves, as on the basal plane, all three modes start at the shear wave velocity of steel and approach the shear wave velocity of PZT-5H. For the Scholte waves, the dispersion curve shows the same trends as that on the isotropic basal plane, starting at the Scholte wave velocity of steel- water interface and approaching that of water-PZT-5H.

For X axis propagation, the electric fields are coupled to the Love waves instead of the Rayleigh waves. Because the dielectric constant of water ($\varepsilon_r = 80$) is higher than that of free space, the dispersion curve of the Love waves is changed from those when the layer surface is traction free. For the $k_r a$ range of 0 to 5, the phase velocities of all the modes are a little lower than those obtained with traction free boundary conditions, Fig. 6. Since the Love waves do not transfer their energy to either water or steel, their wave number k is a real number and the cut-off velocities are the bulk shear wave velocity of steel (v_s). Figure 7 shows $\Delta v / v$ for the first mode Love waves, where it reaches its maximum value at a $k_r a = 2.8$. For the Rayleigh waves, the dispersion curves are similar to those on the basal plane. For loss factors, Fig. 8, the first mode starts at the value of 0.011 and after showing a maximum value at $k_r a = 2.4$, approaches an asymptotic value. The minimum value is located at $k_r a = 0.7$. The Scholte

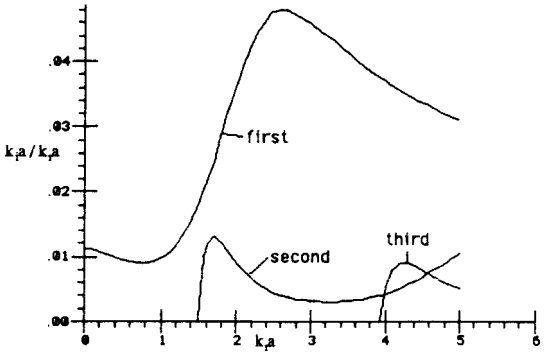

Fig. 5 Loss factor of Rayleigh waves on PZT-5H XZ plane(Z-prop.)

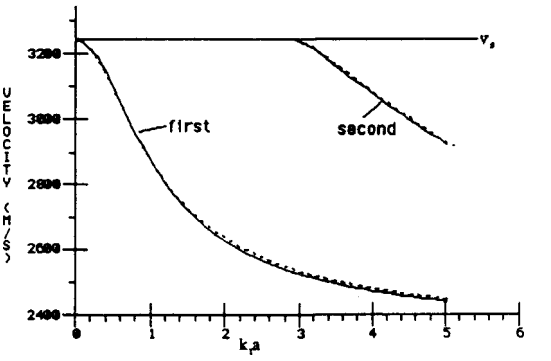

Fig. 6 Dispersion curve of Love waves on PZT-5H XZ plane(X-prop.)

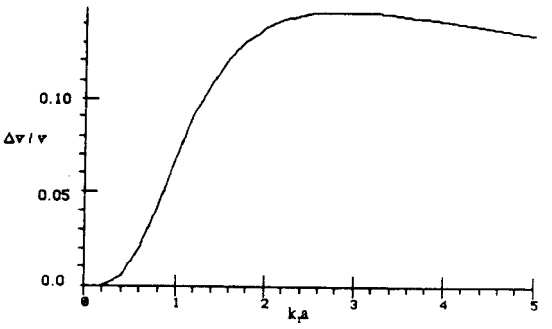

Fig. 7 Excitation efficiency vs. $k_f a$ for first mode Love waves on PZT-5H XZ plane(X-prop.)

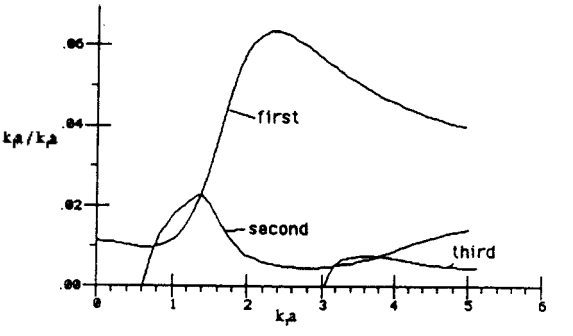

Fig. 8 Loss fractor of Rayleigh waves on PZT-5H XZ plane(X-prop.)

waves also show a similar dispersion curve as before.

Since the crystal XZ plane is anisotropic, the variation of phase velocity as a function of $k_f a$ and propagation direction on the plane is calculated. For the propagation in this plane, a general type of surface waves in which all components of the displacements are coupled to the electric potential is observed. Under these conditions, the Rayleigh and the Love waves do not propagate in pure modes. Figure 9 shows a three dimensional plot for the first mode Rayleigh waves with open circuit boundary conditions, where θ is the angle between the propagation direction and crystal X axis. An angle of 0° indicates X axis propagation and 90° indicates Z axis propagation. For all propagation directions from [100] to [001] on the Y-cut plane, the phase velocity starts at the shear wave velocity of steel and approaches the Rayleigh wave velocity of PZT-5H. With increasing values of θ, the phase velocity smoothly changes from the value for X axis propagation to that for Z axis propagation. To calculate the difference in phase velocities (Δv), a similar figure with shorted boundary conditions at the layer surface is drawn. With these two figures, the excitation efficiency $\Delta v / v$ as a function of $k_f a$ and angle θ is calculated. As shown in Fig. 10, the value of $\Delta v / v$ is significant for X axis propagation but almost negligible for Z axis propagation. The region showing the highest value of $\Delta v / v$ is at $k_f a = 1.4$ and angle $\theta = 22.5°$. But the SAW popagation in this direction is not a pure mode.

Now the crystal cut of the surface plane is

changed gradually from Z-cut to Y cut. Figure 11 shows the three- dimensional dispersion curve of the first mode Rayleigh waves. In the figure, X_1, X_2 and X_3 denote a cartesian coordinate system and X, Y and Z are crystal axes. The angle β is the rotation angle showing the orientation of the surface plane with respect to Y and Z axes. The plane containing the Y, Z, X_1 and X_3 axes is a sagittal plane. In Fig. 11, the crystal cut of the surface plane is changed from Z-cut(angle β=0°) to Y-cut(angle β=90°). For all the rotations, the surface waves propagate in the coordinate X_1 direction on the surface plane. In the other directions on the surface plane, the wave propagation is not a pure mode. Therefore only X_1 direction propagation is considered here. Regardless of the crystal cut, as long as the propagation vector lies in the X_1 dircetion in Fig. 11, it shows the same degenerate case as that on the basal plane. The Rayleigh waves coupled to the electric potential are totally uncoupled from the Love waves. For all the cuts, the starting velocities are the Rayleigh wave velocity of steel. Figure 12 shows the variation of the loss factor of the first mode Rayleigh waves as a function of the rotation angle β and k_Ta. The values of k_Ta showing the minimum and the maximum k_{ia}/k_Ta are different for different cuts but they are aproximately 0.6

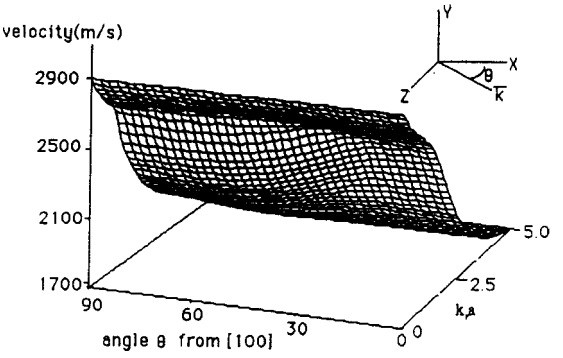

Fig. 9 Velocity vs. k_Ta and angle θ from X axis(Rayleigh -first mode), PZT-5H XZ plane as a surface plane

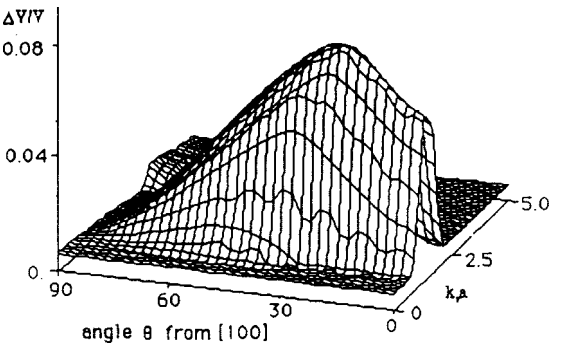

Fig. 10 Excitation efficiency vs. k_Ta and angle θ from X axis
(Rayleigh -first mode), PZT-5H XZ plane as a surface plane

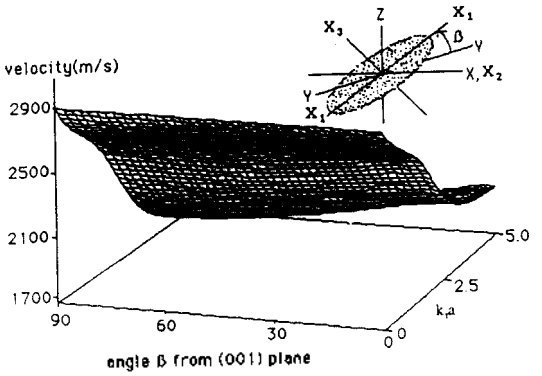

Fig. 11 Velocity vs. k_Ta and angle β from X axis(Rayleigh -first mode)
PZT-5H XZ plane as a sagittal plane

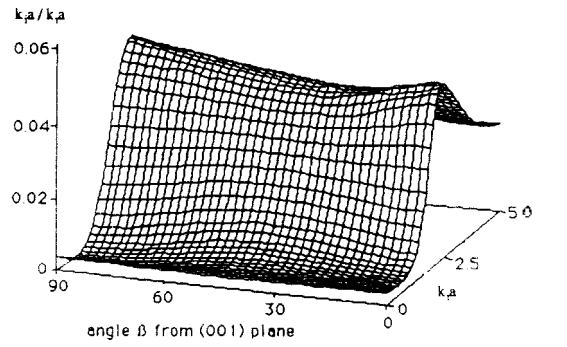

Fig. 12 Loss factor vs. k_Ta and angle β from X axis
(Rayleigh -first mode)
PZT-5H XZ plane as a sagittal plane

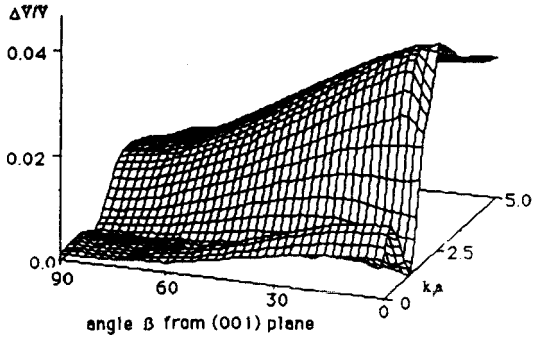

Fig. 13 Excitation efficiency vs. k_ra and angle β from X axis
(Rayleigh first mode), PZT-5H XZ plane as a sagittal plane

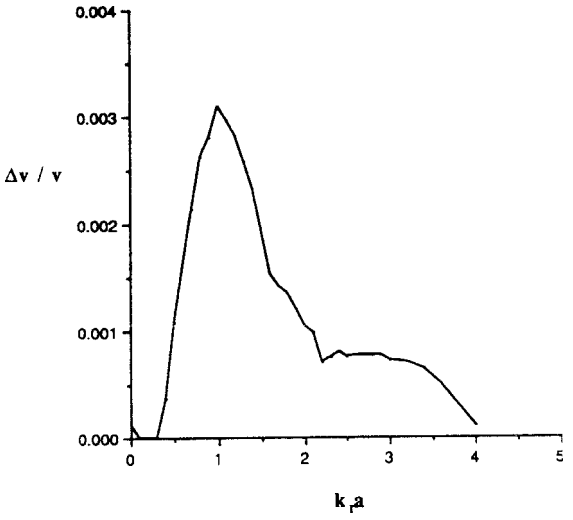

Fig. 14 Excitation efficiency vs. k_ra for first mode Rayleigh waves on PVDF XY plane(X prop.)

and 2.5, respectively. As the cut of the surface plane is changed from Y cut to Z cut, the loss factor increases slowly. For the Love and the Scholte waves also, three dimensional dispersion curves are drawn.

Also, similar curves were drawn with a shorted boundary condition at the [illegible] isotropic basal plane, the phase velocities of Rayleigh waves would be influenced by the short circuit but those of Love waves would not, because the former involves the electric potential but the latter does not. In the same manner, the surface wave excitation efficiency as a function of k_ra and angle β is drawn, Fig. 13. With increase of the rotation algle β, the value of $\Delta v / v$ decreases slowly. With k_ra, it shows a local maximum at around 0.6 and becomes almost 0 at about 1.2. After that, it increases rapidly and reaches another maximum at $k_ra=2.6$. Thus Z-cut crystal, X axis propagation and k_ra value of 2.6 is the most desirable combination to get the highest surface wave excitaion effciency.

So far, the calulation was performed with a PZT-5H layer and a steel substrate. The same technique is applied to the device composed of a PVDF layer and a steel substrate. With the recently measured material properties of PVDF [13], the same numerical analysis is performed. But because PVDF is available only as thin films, only crystal XY plane can be used as the layer of a SAW device. On the XY plane, only crystal X and Y axes are SAW pure mode propagation directions. For the two axes, crystal X axis is preferred because of its higher SAW generation efficiency and low attenuation in propagation. Figure 14 shows the excitation efficiency variation with k_ra of first mode Rayleigh waves on the X axis propagation and it shows the maximum value at $k_ra=1.1$. Similarly, the attenuation rate of the Rayleigh waves on the X axis is calculated and the minimum is at $k_ra=0.9$ as shown in Fig. 15.

Ⅳ. Determination of Optimal Geometry of Underwater SAW Devices

With all the [illegible] the optimal gemoetry of an underwater SAW device with a PZT-5H layer and a steel substrate is determined. In the isotropic basal plane of PZT-5H the value of $\Delta v / v$ for the first mode Rayleigh waves, Fig.

4, reaches a local maximum at $k_ra \simeq 0.6$ and 2.6. The propagation of both the Rayleigh and the Love waves on this plane is pure mode. The variation of the loss factor(k_ia/k_ra) with k_ra is the minimum at $k_ra \simeq 0.6$ for the Rayleigh waves, Fig. 3. For the Love waves, since they are not coupled to the electric field, shorting the free surface has no effect on it.

On the crystal XZ plane, for the Rayleigh waves, the value of $\Delta v/v$ is the maximum at $k_ra \simeq 1.4$ and the propagation direction 22.5° from the crystal X axis to Z axis, Fig. 10. But on this plane, only the X and the Z axis propgation is pure mode and instead of the above value, $k_ra \simeq 1.4$ and X axis propagation is chosen as th optimum. On this axis, the attenuation rate is the minimum at $k_ra \simeq 0.7$, Fig. 8. For the Love waves, $\Delta v/v$ is the maximum at $k_ra \simeq 2.8$ in X axis propagation, Fig. 7.

Finally, for the X_1 direction propagation on different crystal cuts, Fig. 13 shows that $\Delta v/v$ for the Rayleigh waves is the maximum at $k_ra \simeq 0.6$ and 2.6 at Z-cut crystal plane. The wave propagation in the X_1 direction on all the crystal cuts is pure mode. The value of k_ra showing the minimum loss factor is different for different cuts, but it is approximately 0.6 for all the cuts, shown in Fig. 12. For the Love waves, the shorted boundary conditions on the surface does not make any difference.

By comparing these results, for the first mode, the optimal geometry of the underwater SAW device composed of a PZT-5H layer and a steel substrate is determined as : (1) for the Rayleigh waves, all the directions on the isotropic basal plane (Z-cut) of PZT-5H and $k_ra \simeq 0.6$ (2) for the Love waves, X axis propagation on the crystal XZ plane (Y-cut) PZT-5H and $k_ra \simeq 2.8$.

For the SAW device with a PVDF layer and a steel substrate, the optimal geometry is determined in the same manner. With the PVDF XY plane as the layer surface, Fig. 14 shows the excitation efficiency variation with k_ra of first mode Rayleigh waves on the X axis propagation and it show the maximum value at $k_ra \simeq 1.1$. Similarly, the attenuation rate of the Rayleighwaves on the X axis is calculated and the minimum is at $k_r \simeq 0.9$ as shown in Fig. 15. Therefore, from the results, the X axis propagation on the crystal XY plane of PVDF and $k_ra \simeq 1.1$ is determined as the optimal geometry for the Rayleigh waves. For the Love waves, they can be generated by IDTs only in directions between the crystal X and Y axes on the XY plane. But they are not pure mode propagation directions. Thus the PVDF XY plane is not appropriate for the generation of the Love waves.

V. Conclusion

Designing an immersable SAW device requires more attention and full information about underwater surface wave properties due to the leakage of wave energy into water. Therefore, an accurate

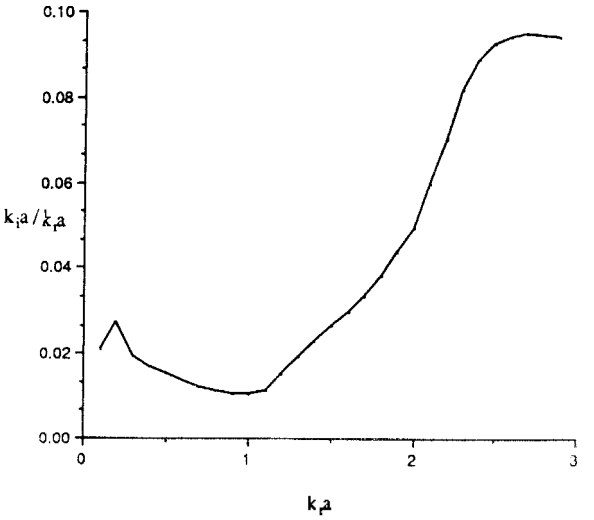

Fig. 15 Loss factor of Rayleigh waves on PVDF XY plane (X prop.)

and reliable design method of the device needs to be developed to overcome the attenuation and get the highest SAW generation efficiency. In this paper, for the development of the technique, detailed propagation properties of all the possibele modes of sur face waves in a layered medium was studied. Based on the results, the opt imal geom etry of underwater SAW devices for each type of surface waves was d etermined to get the minimum attenuation in propagation, the maximum generation efficiency, and pure mode propagation. The optimal geometry includes piezoelectric crystal cut, SAW propagation direction, and nondimensional wave number. Calculation was performed by modeling the underwater SAW device composed of a PZT-5H layer and a steel substrate. Then the developed method was applied to the device composed of a PVDF thin layer and a steel substrate, and its optimal geometry was obtained.

The technique developed here can be generally applied to optimize the geometry of underwater SAW devices using a variety of piezoelectric materials with great accuracy and covenience. The technique can be easily employed for the design of underwater sensors and actuators for the applications, such as sonar[13], marine antifouling[14], industrial and medical uses[15, 16, 17].

REFERENCES

1. V. M. Ristic, "Principles of acoustic devices", John Wiley & Sons, New York, 1983.
2. R. C. Williamson, "Case studies of successful surface acoustic wave devices", IEEE Ultrasonics Symposium, pp. 460~468, 1977.
3. I. A. Viktorov, E. K. Grishchenko and T. M. Kaekina, "An investigation of the propagation of ultrasonic surface waves [sic] Rayleigh [sic] waves [sic] under a liquid", Soviet Physics - Acoustics, Vol. 9, pp. 13 1~137, 1963.
4. J. E. Roederer and G. J. Bastiaans, "Microgravimetric immunoassay with piezoelectric crystals", Analytical Chemistry, Vol. 55, pp. 2,333~2,336, 1983.
5. G. J. Bastiaans and C. M. Good, "Developement of a surface acoustic wave biosensor", Transducers '8 7 Digest, pp. 424~429, 1987.
6. J. J. Campbell and W. R. Jones, "A method for estimationg optimal crystal cuts and propagation directions for excitation of piezoelectric surface wav es", IEEE Transactions on Sonics and Ultrasonics, Vol. SU 15, pp. 71~76, 1968.
7. B. A. Auld, "Acoustic Fields and Waves in Solids", Vol. I 2, John Wiley, New York, 1973.
8. H. Uberall, "Surface waves in acoustics", Physical Acoustics W. P. Mason and R. H. Thurston (eds), Academic Press, Vol. 10, pp. 1~60, 1972.
9. W. M. Ewing, W. S. Jardetzky and F. Press, "Elastic Waves in Layered Media", McGraw Hill, New York, 1957.
10. Y. R. Roh, V. V. Varadan, V. K. Varadan and R. H. Tancrell, "Measurement of all the elastic and dielectric constants of poled PVDF filme", IEEE Ultrasonics Symposium, 1989.
11. G. W. Farnell, "Properties of elastic surface waves", Physical Acoustics, W. P. Mason and R. H. Thurston (eds.), Academic Press, Vol. 6, pp. 109~166, 197
12. J. J. Campbell and W. R. Jones, "Propagation of surface waves at the boundary between a piezoelectric crystal and a fluid medium", IEEE Transactions on Sonics and Ultrasonics, Vol. SU-17, pp. 7 1~76, 1970.
13. Y. R. Roh, V. V. Varadan, V. K. Varadan and R. H. Tancrell, "Measurement of all the elastic dielectric and piezoelectric constants of poled PVDF films", IEEE Transactions on Ultrasonics, Ferroelectrics and Frequency Control (to be pressed).
14. Y. R. Roh, V. V. Varadan and V. K. Varadan, "Application of surface acoustic waves for marine fouling prevention", 119th Meeting of Acoustical Society of America, the Pennsylvania State Unive rsity, PA, May 1990.
15. V. V. Varadan, Y. R. Roh and V. K. Varadan, "Local, Global SAW sensors for turbulence", Proce edings of Ultrasonics Symposium, Oct. 1989.
16. Y. R. Roh, V. V. Varadan and V. K. Varadan, "Local-Global SAW sensors for turbulence-II", Jou rnal of Wave and Material Interaction, Dec. 1989.
17. V. V. Varadan, Y. R. Roh, X. Q. Bao, T. R. How arth and V. K. Varadan, "Composite smart skins for airborne structures", Proceedings of SPIE- the

International Society for Optical Engineering (Society for Photo- Optical Instrumentation Engineers), in the OE / Aerospace Sensing Meeting under Electro Optic Materials for Switches, Coatings, Sensor Optics and Detectors, Orlando, Florida, April 1990

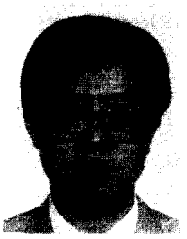

Yongrae Roh received the B.S. and M.S. degrees in Mineral and Petroleum Engineering from the Seoul National University, Seoul, in 1984 and 1986, respectively. He got the Ph.D. degree in Engineering Science and Mechanics (major in Acoustics) from the Pennsylvania State University, U.S.A., in 1990. He is currently a senior research scientist in the Research Institute of Industrial Science and Technology, Pohang. Major research area includes SAW devices, ultrasonic transducers, NDT and noise & vibration control. He received the "Oustanding Ph.D. student research award" from the Pennsylvania State University in 1989 and the 1990 Xerox Award, U.S.A., for the best research in materials.